Spatial Maps of Krypton Neutral Density in SPT-70 HET Plume by TALIF

IEPC-2025-218

Presented at the 39th International Electric Propulsion Conference Imperial College London • London, United Kingdom 14-19 September 2025

Jon Stienike¹, Matteo Da Valle², Mitchell Morasco¹, Seth Thompson³, John D. Williams⁴, and Azer P. Yalin⁴

Colorado State University, Fort Collins, CO, 80523, U.S.A

Abstract

This work presents the first high-resolution spatial maps of neutral density in the near-field plume of a Hall effect thruster (HET) using two-photon absorption laser-induced fluorescence (TALIF). We employed a 212.6 nm TALIF excitation scheme to map krypton neutral densities in the plume of a Fakel SPT-70 sub-kilowatt thruster. The diagnostic system incorporated active wavelength stabilization via a feedback-controlled dye laser and comprehensive drift correction algorithms to maintain measurement accuracy through extended mapping campaigns due to drifts in laser performance. Systematic error analysis through controlled validation experiments established an overall measurement uncertainty of ~20%. Neutral density maps were acquired under cold-flow conditions and four plasma operating states (540W and 720W at varying background pressures), highlighting the effects of power level and background pressure on the nearfield neutral particle profile. These results provide crucial experimental benchmarks for validating computational models and advancing physical understanding of neutral behavior in electric propulsion devices.

I. Motivation and Background

Compared to traditional chemical propulsion, electric propulsion (EP) devices utilize propellant mass much more efficiently due to their higher specific impulses [1,2]. Among EP technologies, Hall-effect thrusters (HETs) have become especially attractive for both commercial and scientific missions, offering high thrust efficiency and substantial ΔV capability. In HETs, thrust is generated by ionizing a neutral propellant, typically xenon, krypton, or argon, and accelerating the resulting ions to high velocities ($\sim 10-80 \text{ km/s}$) using crossed electric and magnetic fields [1]. The complex plasma dynamics that emerge under these conditions give rise to instabilities that directly affect thruster performance and lifetime [3]. Developing diagnostic techniques to characterize both plasma instabilities and neutral distributions is therefore essential for validating models, improving predictive capability, and guiding the design of next-generation thrusters.

Neutrals play a critical role in nearly every aspect of HET operation. They participate in charge-exchange (CEX) reactions that modify the ion energy distribution in the plume [4,5]. The neutral density profile also influences anode efficiency through background gas ingestion, while mismatches in neutral density between ground-based facilities and on-orbit conditions contribute to facility effects [4]. In vacuum chambers, background pressures are typically on the order of 10^{-4} – 10^{-6} Torr, whereas true space conditions can reach $\sim 10^{-12}$ Torr. This disparity leads to elevated neutral densities in laboratory environments, artificially enhancing CEX rates and altering plume properties such as divergence and ion energy spread [4]. Accurate characterization of neutral distributions is thus critical for decoupling facility-driven artifacts from intrinsic thruster physics.

⁴ Professor, CSU – ME, John.D.Williams@colostate.edu, Azer.Yalin@ColoState.EDU



¹ Graduate Research Assistant, Colorado State University (CSU) – Mechanical Engineering (ME), jon.stienike@colostate.edu, Mitchell.Morasco@colostate.edu

² Post Doctoral Researcher, CSU - ME, matteo.davalle@colostate.edu

³ Research Scientist, CSU - ME, <u>Seth.Thompson@colostate.edu</u>

Direct measurements of neutrals using physical probes are limited in scope and accuracy. Pitot-tube style probes, for example, can measure static pressure that may be related to number density through the ideal gas law [6]. However, such probes inherently perturb the rarefied flow field and are poorly suited for capturing the strongly non-equilibrium conditions of EP plumes. Their intrusion can alter the very neutral distributions they attempt to measure, and probe survivability is further challenged by the high-energy ion environment near the thruster. These shortcomings underscore the need for non-intrusive diagnostic approaches capable of providing localized, quantitative neutral measurements.

Two-photon absorption laser-induced fluorescence (TALIF) has emerged as a leading non-intrusive diagnostic for neutral density measurements. TALIF enables ground-state detection by exciting neutrals through a two-photon transition to an upper electronic state, which subsequently emits fluorescence as it decays. This technique is particularly well-suited to noble gases such as xenon and krypton, whose ground states cannot be accessed via single-photon excitation at available UV wavelengths. TALIF offers high sensitivity and spatial resolution while avoiding the flow disruption inherent to probes.

Several groups have advanced the development of TALIF for electric propulsion applications. Pioneering work by Crofton demonstrated Xe TALIF in the plume of the T5 ion thruster, while Eichhorn et al. extended the approach to Kr in both gridded and RF ion thrusters [7–10]. More recently, Crofton has also applied TALIF to study Xe in the plume of an SPT-140, capturing broad neutral distributions with relatively coarse spatial resolution [11]. Building on this foundation, TALIF has since been applied to map Xe and Kr neutral densities in cathode and Hall thruster plumes, and more recently to incorporate temporal resolution for capturing neutral dynamics associated with the breathing mode instability in a 1.5 kW Hall thruster [12–15]. The breathing mode, a predator–prey type oscillation between ionization and neutral replenishment, manifests as strong, coherent fluctuations in discharge current at ~10–30 kHz [16,17]. Although identified nearly 50 years ago, it remains an active area of research, particularly given the risks that large-amplitude oscillations can pose to on-orbit systems. Demonstrations of temporally resolved TALIF have shown that the technique can provide unique insights into neutral oscillations during this instability [15].

Despite these advances, quantitative high-resolution spatial mapping of neutral densities in HETs has been limited. Prior efforts, such as Crofton's SPT-140 study, established broader neutral distribution trends but did not capture fine structure. Yet such measurements are essential: even under cold-flow conditions, they provide valuable data for informing models of neutral injection, plume expansion, and CEX reaction locations. Without experimental benchmarks, simulations often rely on simplified assumptions regarding neutral distributions. High-resolution experimental measurements are therefore crucial for improving predictive capabilities and optimizing neutral injection strategies. In this work, we present the first high-resolution spatial maps of neutral density in the near-field plume of a HET. These results establish new experimental benchmarks for validating models and advancing the physical understanding of neutral behavior in EP devices. The layout for the remainder of the paper is as follows. Section II describes experimental setup and methods. Section III provides results and discussion, while Section IV provides conclusions and avenues for future work.



II. Experimental Setup and Methods

A. Optical Scheme

This work employs two-photon absorption laser-induced fluorescence (TALIF) using a 212.6 nm excitation scheme with detection at 758.7 nm, as shown in Fig. 1, following our past Kr TALIF work. Two 212.6 nm photons are simultaneously absorbed by ground state neutral Kr (4p⁶ ¹S₀). This excites it to the 5p ²[1/2]₀ level which will then decay into one of two levels, 5s ²[1/2]⁰₁ or 5s ²[1/2]⁰₁ emitting at 1212.4 and 758.7 nm respectively. We collect the latter. These will then further decay back to the ground state. While no saturation curves were experimentally determined with this setup, we confirmed that we were measuring in the linear regime where an increase in laser energy leads to a proportional increase in TALIF signal.

B. Experimental Setup

The optical setup is shown in Fig. 2. The UV probe laser source is a nanosecond pulsed dye laser (Sirah Precision Scan) pumped by the third harmonic (355 nm) output of an

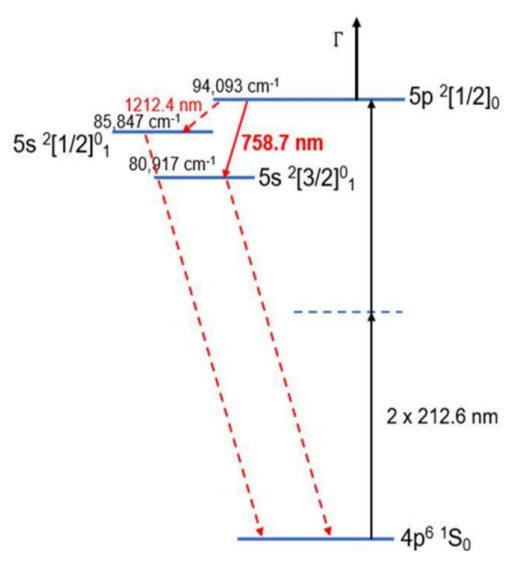


Figure 1. TALIF excitation scheme.

Nd:YAG laser (Spectra-Physics Quanta Ray Lab 150-10) with a pulse energy and duration of ~150 mJ and 9 ± 1 ns at half-maximum (FWHM). The dye laser uses a diluted concentration of Exalite 428 dye to produce visible light at 425 nm with a linewidth of ~1.7 pm which is then doubled using an integrated frequency conversion unit (FCU) to the required 212.6 nm light at 1.8 mJ needed to induce TALIF. The probe beam is directed from the dye laser by two UV fused silica (UVFS) turning prisms arranged in a periscope fashion to steer the beam through a 1.5" UVFS vacuum rated window. As we operate in the linear regime for TALIF, a photodiode measures the intensity of the probe beams reflection off the steering prisms to allow for energy normalization. Once the beam passes into the vacuum chamber, a 300 mm lens focuses the beam to a weak focus at a point downstream of the exit plane of the thruster face, as shown in Fig. 3, where high enough photon density permits a measurable TALIF signal. At an angle perpendicular to the probe beam, a 300 mm plano convex lens collects and then collimates the TALIF signal, along with the plasma's luminous emission from this point. This collimated light is then coupled into a 600 µm fiber optic cable with a 150 mm lens, delivering the TALIF light to a Hamamatsu R3896 photo multiplier tube (PMT) equipped with a narrow bandpass filter (Thorlabs M29L02) to remove most of the plasma emission that originates at other emission lines as opposed to 760 nm. However, a strong emission line near 761 nm still passes through the filter and contributes significantly to the background luminosity, accounting for roughly 40% of the signal.

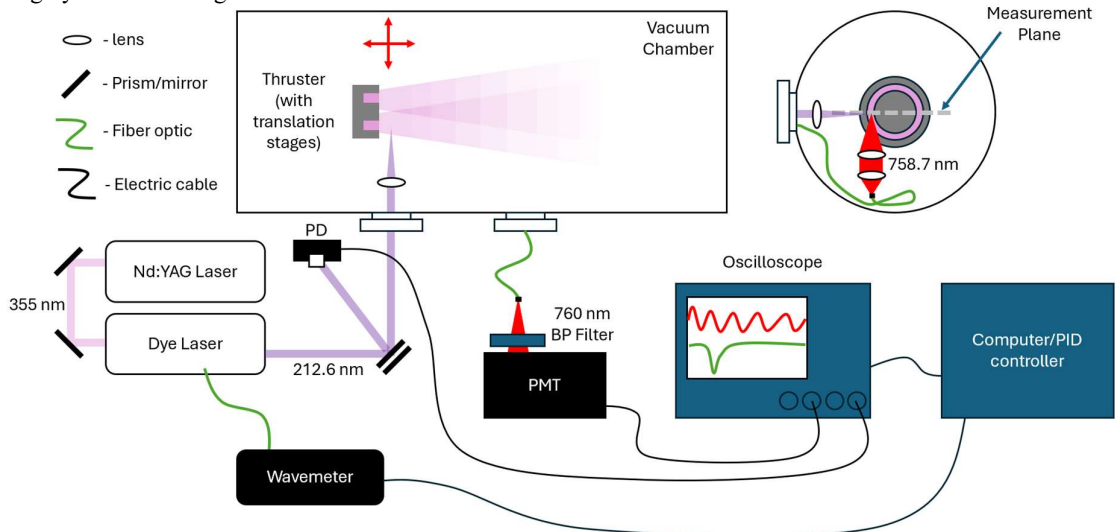


Figure 2. Diagram of TALIF experimental setup, top and front views.



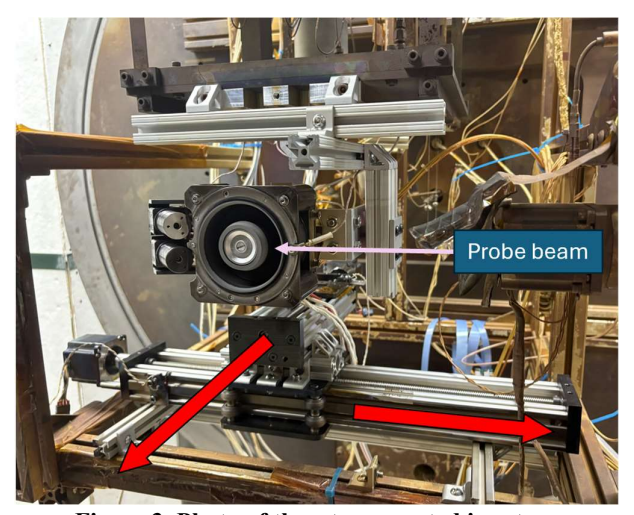


Figure 3. Photo of thruster mounted in setup.

While offering the tunability and power levels necessary for TALIF measurements, dye lasers are known to suffer from gradual drifts in both output wavelength and pulse energy. Over the course of operation, the lasing wavelength can shift due to mechanical and thermal instabilities in the lasing cavity, while the pulse energy deteriorates as a result of dye conditioning as well as due to environmental conditions. To address the issue of wavelength drift, a HighFinesse WS5 wavemeter was incorporated into the setup to measure the fundamental frequency of the dye laser prior to frequency doubling. This signal was then used in a feedback loop with a PID controller via a Sirah Control software plugin to actively stabilize the laser wavelength. In parallel, a fast photodiode was installed to monitor the relative intensity of each laser pulse. While the wavemeter counteracted wavelength drift in real time, the photodiode traces of the laser intensity provided a way to correct for fluctuations and drifts in pulse energy during post processing by normalizing each TALIF signal trace to the corresponding pulse energy.

Environmental conditions presented additional challenges. The laboratory space where TALIF was performed lacked HVAC control, leading to large temperature swings throughout the day. These fluctuations were influenced both by outside weather conditions and by the significant heat load generated by high-power laser power supplies and other equipment. Since dye lasers are particularly sensitive to temperature variations, these drifts in both output wavelength and pulse energy made the ambient environment untenable. To mitigate this, we built a small enclosure around the laser system and cooled it using two portable air conditioning units. This localized thermal regulation provided a more stable environment for laser operation, reducing environmental contributions to drift and improving both the reproducibility and accuracy of TALIF measurements.

All testing took place in the Orion chamber at the Center for Electric Propulsion and Plasma Engineering laboratory at Colorado State University, a 1.7 m diameter, 4.6 m long cylindrical vacuum chamber outfitted with a roughing pump, two diffusion pumps, and two cryo-sails, providing a nominal pumping speed of \sim 17,000 L/s on Kr and maintaining a background pressure of approximately 9x10-7 Torr. Neutral density measurements were obtained under both cold-gas flow through the anode and the cathode as well as four primary plasma-operating conditions for different power levels and background pressures as shown in Table 1 to highlight the effects of both power and pressure.

C. Data Acquisition

As can also be seen in Fig. 2, the data acquisition was carried out using a digital phosphor oscilloscope (Tektronix TDS 5034B), which simultaneously recorded the TALIF signal and the photodiode trace for each laser shot. The oscilloscope was externally triggered by the Q-switch signal from the Nd:YAG laser power supply to ensure consistent temporal alignment across all measurements. At each spatial location in the plume, 500 individual laser shots were collected, providing sufficient statistics to account for both laser fluctuations and plasma variability. The TALIF signal and corresponding photodiode reference were stored for each shot, enabling normalization of the fluorescence signal by pulse energy during post-processing. In parallel, the wavemeter (HighFinesse WS5) continuously monitored the dye laser wavelength and provided feedback to the PID controller for active stabilization. All instruments, including the oscilloscope, wavemeter, and control electronics, were interfaced with



a central computer running a LabVIEW VI that handled data logging and coordination of the acquisition sequence as well as the PID controller for the wavelength stabilization.

D. Thruster Mounting and Translation Stages

The HET to be used in this study is a Fakel SPT-70, a sub-kilowatt-class thruster. The HET is mounted on a thrust stand equipped with a two-dimensional motion stage, allowing precise axial and radial movement allowing measurement of a 2D neutral density map in the same plane as the UV probe beam that intersects the centerline of the thruster. This allows for the alignment of the probe beam and collection optics to remain focused at a fixed location while the thruster moves relative to that. The translation stages are moved by a fine 2 mm step sizes close to the thruster to capture the steep gradients in neutral density due to the expansion of the flow into the chamber. The gradients decrease as the density approaches the background pressure in the chamber, allowing for larger spacing between measurement locations to effectively capture the neutral density profile in the near field plume. Fig. 4 shows the coordinate system used in this study.

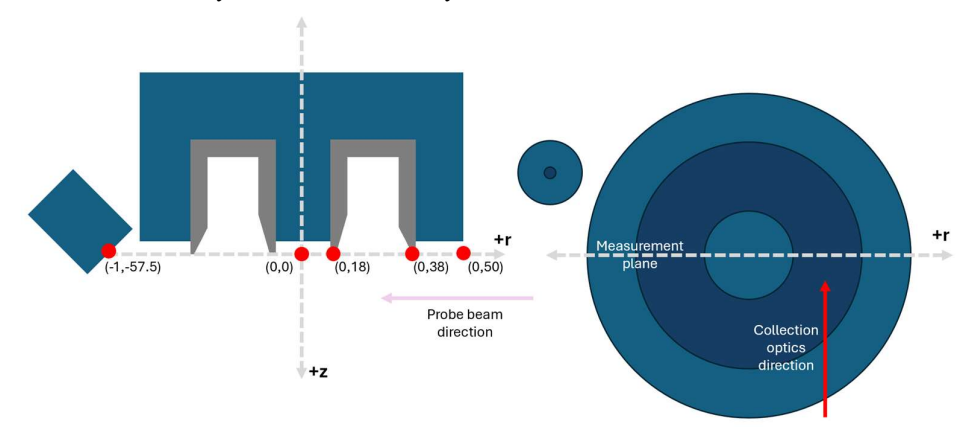


Figure 4. Top and front views of a cross sectional cut of the HET with the measurement coordinate system, (z,r), in mm.

The spatial maps presented in this study are constructed from measurements collected on a non-uniform grid of points, which creates inherent challenges for data visualization and interpretation. To address the gaps between measured points and generate continuous spatial representations, we developed a weighted nearest neighbor averaging algorithm that interpolates values for locations with no measurements. This algorithm identifies data points that bracket each interpolation location in both radial and axial directions, assigning weights based on the inverse distance to the point of interest. While this interpolation approach provides smooth visual representations, it may not fully capture the underlying physics governing the spatial distributions, potentially leading to minor deviations from the actual physical behavior in regions between measurement points. However, these limitations are largely mitigated by our strategic selection of measurement locations, where we deliberately choose a denser mesh of points in regions exhibiting higher spatial gradients, ensuring that the interpolation occurs over smaller distances in areas where the profiles vary most rapidly.

E. Conversion to Absolute Number Density

The conversion from relative TALIF signals to absolute neutral number densities employs a reference-based calibration approach that accounts for both initial signal scaling and temporal drift corrections. Prior to each mapping sequence, the measurement system is positioned laterally and downstream of the HET thruster, well outside the neutral expansion region to avoid contamination from thruster-generated density gradients. At this reference location, approximately 1 meter behind the thruster, a controlled flow of the target neutral species is released through a bleed line while the chamber background pressure is monitored at 1.2×10^{-4} Torr as measured by an ion gauge situated 1 meter behind the thruster on the opposite side of the chamber. The ion gauge has a 15% error in the absolute measurement as well as a 5% repeatability error. The initial TALIF signal collected at this known pressure condition is used to establish the absolute calibration factor by calculating the corresponding neutral number density from the measured pressure using the ideal gas law. This reference measurement provides the fundamental scaling relationship between measured fluorescence intensity and absolute particle density.



F. Drift Correction Methodology

To maintain measurement accuracy throughout the experimental campaign, a two-stage drift correction protocol is implemented to compensate for wavelength instabilities inherent to the wavemeter's limited resolution. Immediately following thruster ignition and thermal stabilization, a new reference signal is acquired at the same calibration location, establishing the operational scaling factor that accounts for any systematic changes in the optical system or neutral flow conditions. During plume mapping, periodic returns to this reference position occur every 5-10 measurement points to monitor signal drift over time. The temporal evolution of these reference signals is fitted with a linear function, and this time-dependent correction factor is applied to all plume measurements taken between any two reference points. This methodology ensures that the final number density maps better reflect true spatial variations in neutral particle concentration rather than artifacts from instrumental drift, providing quantitatively accurate neutral density profiles throughout the HET near-field plume region.

G. SPT-70 Operating Conditions for Testing

To investigate how power and background pressure influence the near-field neutral profiles of the SPT-70, we selected four primary plasma conditions for testing, summarized in Table 1. Specifically, we performed TALIF measurements at two discharge power levels, 540 W and 720 W, each tested at two background pressures of approximately 30 μ Torr and 60 μ Torr. This experimental matrix allowed us to make direct comparisons between the two power levels, as well as to assess the impact of elevated background pressure at each power setting. In this way, we could decouple the effects of discharge power and facility pressure on neutral dynamics in the near-field plume. The left side of Fig. 5 shows a photograph of the SPT-70 operating on krypton under these test conditions.

Condition	Test Type	ṁа	ṁс	PD	VD	ID	P
		(SCCM)	(SCCM)	(W)	(V)	(A)	(µTorr)
1	Cold flow	27.5	0	-	-	-	25
2	Cold flow	0	3.0	-	-	-	3
3	Plasma	27.5	3.0	540	300	1.8	30
4	Plasma	27.5	3.0	555	300	1.85	60
5	Plasma	34.5	4.0	720	300	2.4	36
6	Plasma	34.5	4.0	735	300	2.45	60

Table 1. The different operating conditions neutral density profiles were measured.

The right side of Fig. 5 presents the power spectra of the discharge current oscillations for each of the four operating conditions. Our approach was to complete all TALIF measurements at a given condition before moving on to the next, thereby minimizing any errors that could arise from restarting the thruster. Throughout testing, we monitored the oscillation spectra of the discharge current to ensure the thruster remained in a consistent mode of operation. This verification was important, as mode transitions could introduce additional variability in the neutral density measurements, making it difficult to isolate the effects of power and pressure.

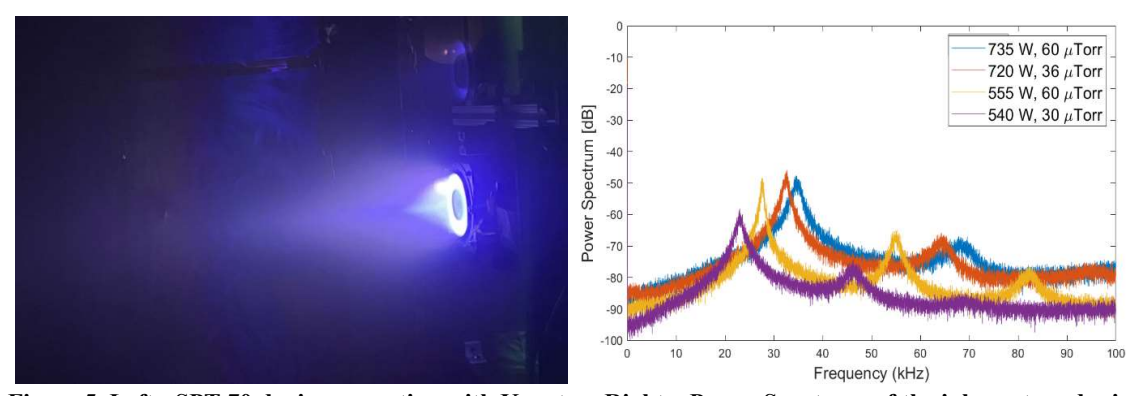


Figure 5. Left - SPT-70 during operation with Krypton. Right – Power Spectrum of the inherent modes in plasma operating condition of interest.

H. Systematic Error Estimation Methodology

In order to truly understand the systematic errors of this experimental campaign, a variety of tests were conducted to isolate sources of error and their impact on the absolute neutral density measurements. Given the complexity



of the TALIF diagnostic system and the challenging measurement environment within the HET plume, multiple potential error sources could contribute to uncertainty in the final density maps, including spatial non-uniformities in the reference calibration region, temporal drift in the laser system, thruster operational repeatability, and mechanical positioning uncertainties. A systematic approach was therefore implemented to characterize each of these error sources independently, allowing for quantitative assessment of their individual contributions to the overall measurement uncertainty and validation of the correction methodologies employed throughout the experimental campaign.

Collectively, these systematic studies, combined with the statistical analysis of measurement repeatability and the propagation of uncertainties from pressure measurements and laser power fluctuations, indicate that the overall systematic error in the absolute neutral density measurements is estimated to be $\sim 20\%$.

III. Results and Discussion

A. Drift Correction Results

The counter drift correction algorithm demonstrates clear effectiveness in improving measurement consistency and data quality across different experimental configurations. Fig. 6 illustrates this improvement through axially resolved TALIF measurements collected at the channel midpoint, directly opposite the externally mounted cathode assembly under condition 3 (540W, 30 μ Torr background pressure). The left panel presents uncorrected data comparing two datasets: the "normal" dataset from comprehensive full map measurements and the "axial" dataset collected immediately afterward along only the channel centerline. In these uncorrected measurements, the error bars (representing standard deviation) become smaller at downstream locations but fail to overlap between the two datasets, indicating systematic disagreement that suggests the presence of drift effects during the measurement period.

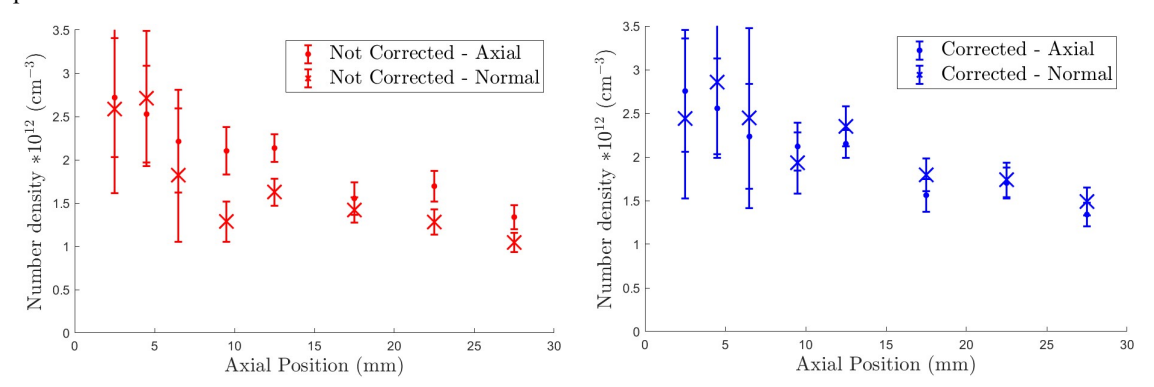


Figure 6. Left – Axially resolved TALIF measurements at the channel midpoint for condition 3 (540W, 30 μ Torr) showing uncorrected data between sequential datasets. Right - Drift-corrected axially resolved TALIF measurements at the channel midpoint for condition 3

The right panel of this figure reveals the substantial improvement achieved through drift correction. After applying the correction algorithm, the error bars between the two measurement sets overlap at every axial location, demonstrating excellent agreement between datasets that were collected at different times. This overlap indicates that the correction successfully reduces the systematic drift that was causing apparent differences between measurements of the same physical conditions. The transformation from non-overlapping to overlapping error bars provides evidence that the counter drift correction effectively limits time-dependent systematic errors while preserving the underlying physical measurements.



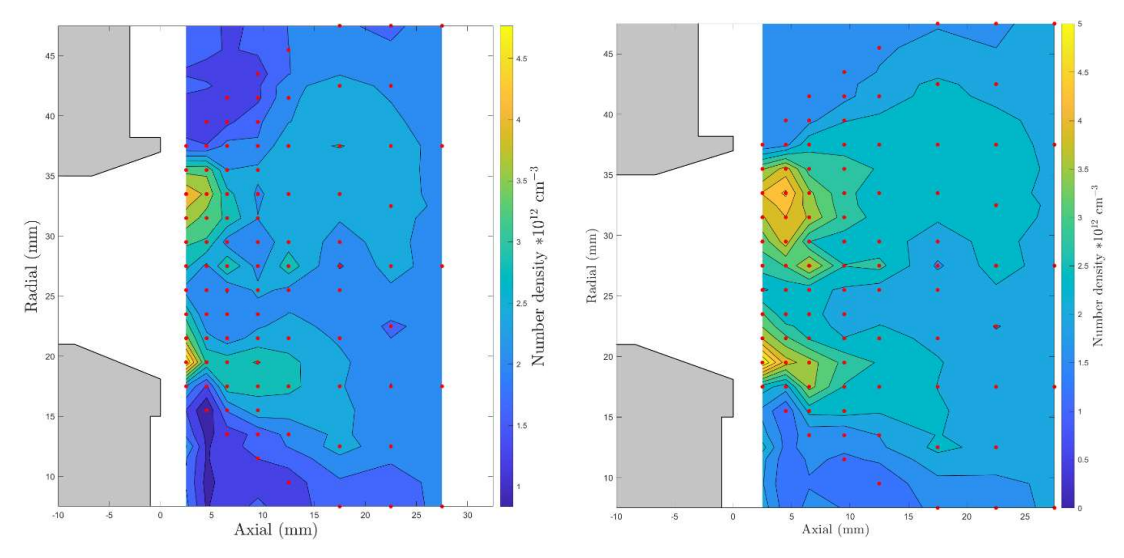


Figure 7. Left – Uncorrected maps of near-field plume neutral density maps for condition 6 (720W, 60 μTorr). Right – Corrected maps of near-field plume neutral density maps for condition 6.

Further validation of the correction algorithm's effectiveness is provided by the full spatial mapping results shown in Fig. 7, which presents neutral density measurements in the near-field plume under condition 6 (720W, 60 μ Torr background pressure). The uncorrected map in the left panel exhibits several problematic features characteristic of drift-contaminated data, including random spatial holes that lack physical justification and regions with artificially suppressed density values. These artifacts arise because the drift consistently reduces the apparent TALIF signal below its true value, creating systematic underestimation that varies unpredictably across the measurement sequence. The corrected map in the right panel shows a marked improvement, with the random holes effectively filled in and a more physically consistent density distribution throughout the measurement domain. This dramatic improvement in spatial data quality demonstrates that the drift correction algorithm not only improves point-to-point measurement accuracy but also restores the physical coherence of complex spatial datasets.

The results presented in this section clearly demonstrate the effectiveness of the counter drift correction algorithm in eliminating systematic time-dependent errors and restoring physical consistency to TALIF measurements. The correction method successfully addresses drift-induced artifacts that would otherwise compromise data quality, as evidenced by the improved agreement between sequential datasets and the elimination of spurious spatial features in density maps. Given these improvements in measurement accuracy and reliability, all subsequent figures and results reported in this study have been processed using this drift correction methodology.

B. Cold Flow Condition Maps

Cold flow measurements provide crucial insight into the natural expansion characteristics of neutral propellant as it exits the thruster channels, free from the complex interactions present during plasma operation. Fig. 8 presents the neutral density distribution for flow exiting the anode on the side opposite the cathode assembly as shown in the accompanying map (condition 1), with measurements beginning 2.5 ± 0.5 mm downstream of the thruster exit plane. The precise measurement locations are indicated by the red dots overlayed onto the map.

The map reveals a distinct asymmetric expansion pattern that can be readily explained by the thruster's geometric design. The discharge channels feature chamfers on both the inner and outer ceramic inserts, with the inner chamfer being significantly more pronounced. This geometric asymmetry causes the neutral flow to preferentially expand toward the thruster axis, creating the observed directional bias in the density distribution.

Fig. 9 shows the complementary cold flow measurement from the cathode side of the thruster (condition 2), where flow originates solely from the cathode assembly rather than the anode, with both conditions representing the neutral flow rates corresponding to the 540W operational state. These comparative cold flow maps establish the baseline asymmetric flow pattern across the thruster face and provide important predictive insight for plasma operation: since the cathode introduces additional propellant flow that remains largely unionized, we expect to observe higher neutral densities on the cathode side compared to the opposite side during plasma conditions.



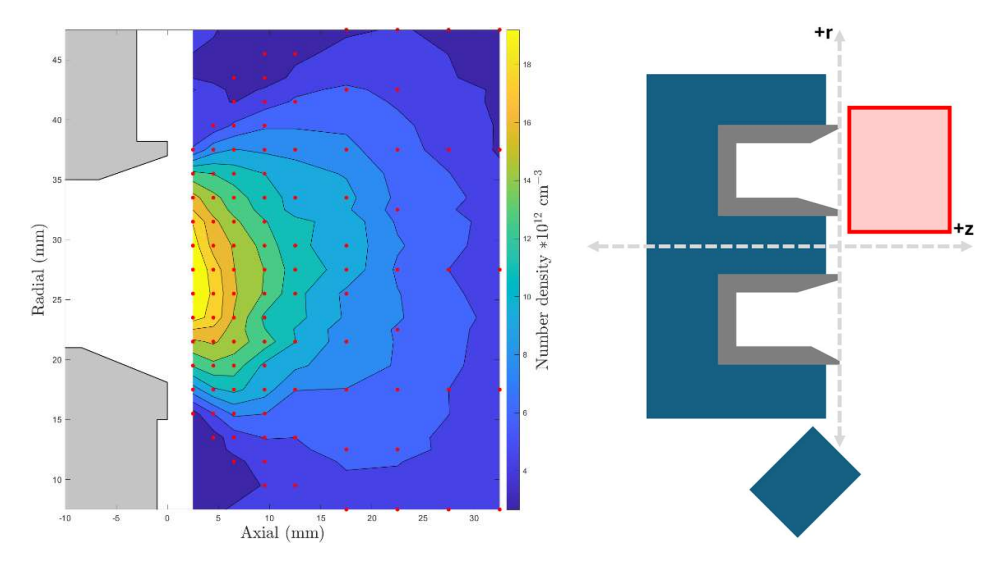


Figure 8. Left - Cold flow neutral density map from anode flow on the side opposite the cathode assembly (condition 1). Right – Region of thruster plume measured by TALIF for the anode-side, anode flow map (highlighted in red).

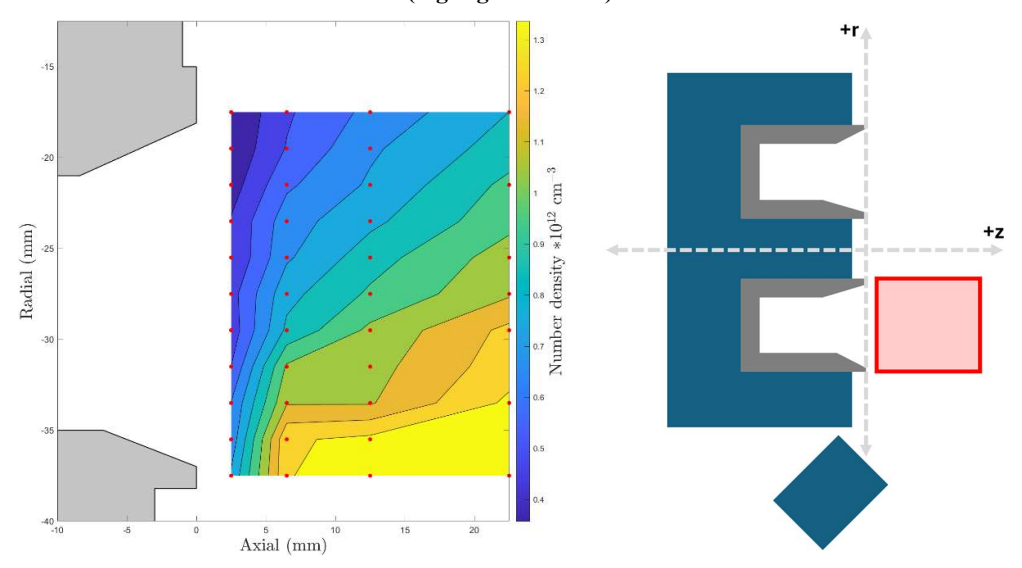


Figure 9. Left - Cold flow neutral density map from cathode-side flow only (condition 2). Right – Region of thruster plume measured by TALIF for the cathode-side, cathode flow map (highlighted in red).

Fig. 10 presents the corresponding measurement uncertainties for the maps expressed in number density units, revealing important characteristics of the TALIF measurement precision under these conditions. In the high-density cold flow environment shown in the left panel, where neutrals flow directly from the anode, the absolute error scales roughly proportionally with the local neutral density. However, the relative uncertainty remains consistently around 2 percent throughout the measurement domain, reflecting the exceptionally high signal-to-noise ratio achieved under these favorable conditions.



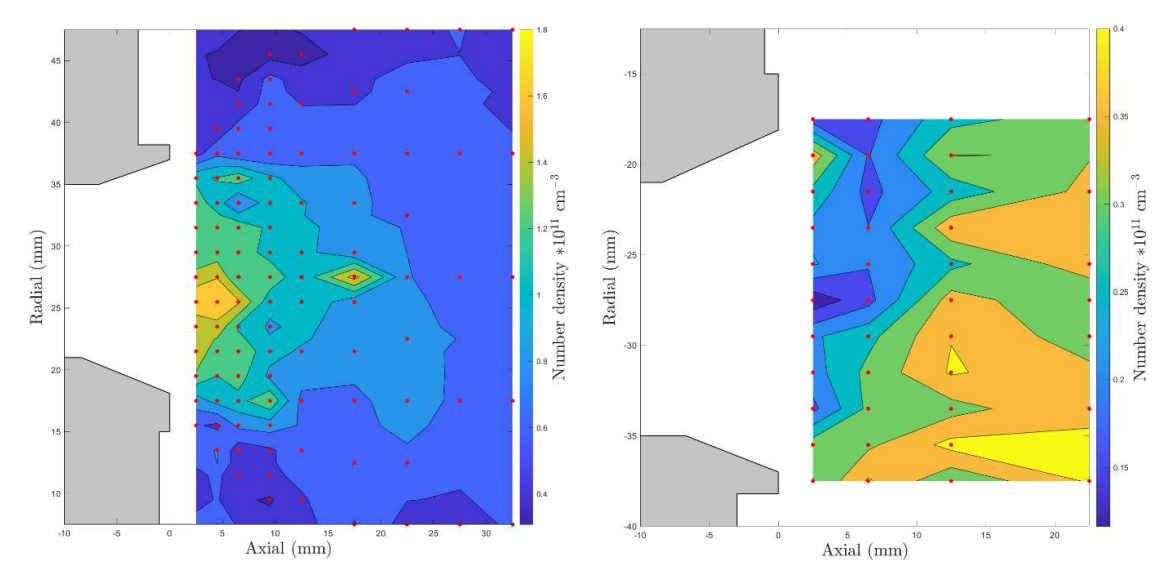


Figure 10. Left – Standard deviation in measurements of anode cold flow map reported in number density. Right – Standard deviation in measurements of cathode cold flow map

This precision results from the combination of high neutral densities and the absence of competing background luminosity that would otherwise degrade measurement quality. These error levels represent a best-case scenario that cannot be expected to be maintained during plasma operation, where neutral densities are expected to decrease by approximately an order of magnitude due to ionization processes, while simultaneously introducing significant background luminosity that will substantially reduce the signal-to-noise ratio and increase measurement uncertainties.

C. Plasma on Condition Maps

The neutral density measurements in the near field plume were conducted across four distinct operational conditions to systematically investigate the effects of discharge power and background pressure on the spatial distribution of neutral propellant. These conditions encompassed both low power (540W) and high power (720W) operations at corresponding low and high background pressures, providing a comprehensive matrix for understanding how these key parameters influence neutral density profiles in the thruster's immediate downstream region.

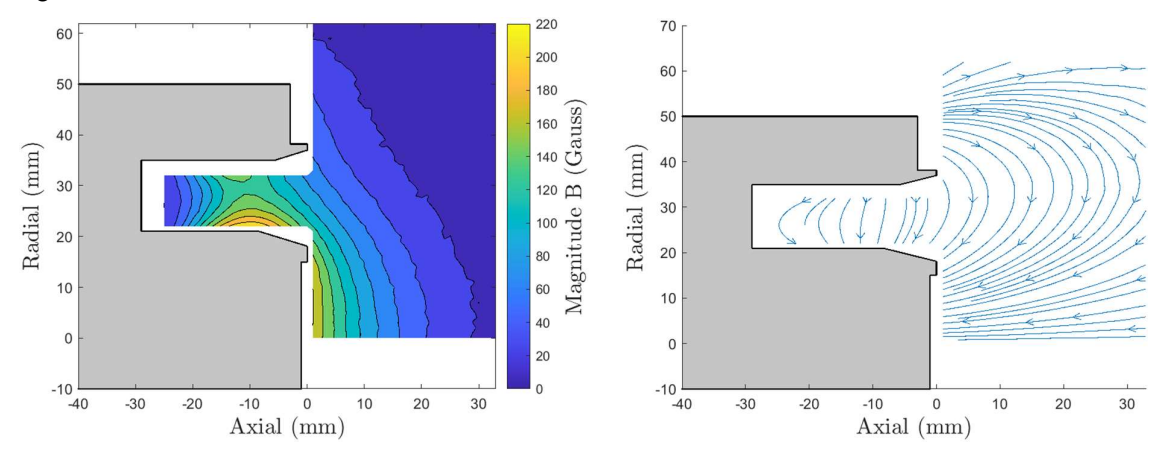


Figure 11. Left – Total Magnetic field strength in SPT-70. Right – Direction of magnetic fields in SPT-70.

The panels of Figs. 12 and 13 present these measurements with the first displaying results from the low power 540W condition at both pressure levels, while the latter shows the corresponding high power 720W measurements for same location Fig. 8 was measured. Across all operational conditions, a consistent spatial pattern emerges characterized by regions of elevated neutral density along the inner and outer edges of the channel walls, separated by a central region of notably lower density. This characteristic "double-peaked" structure with a central depletion zone reflects the fundamental physics of HET operation, where ionization processes occur most intensively in the



central channel region near the inner wall (region of strong magnetic field), consuming neutrals and creating the observed density minimum. To help explain the neutral depletion along the center of the jet, the magnetic field strengths and profile are shown in Fig. 11.

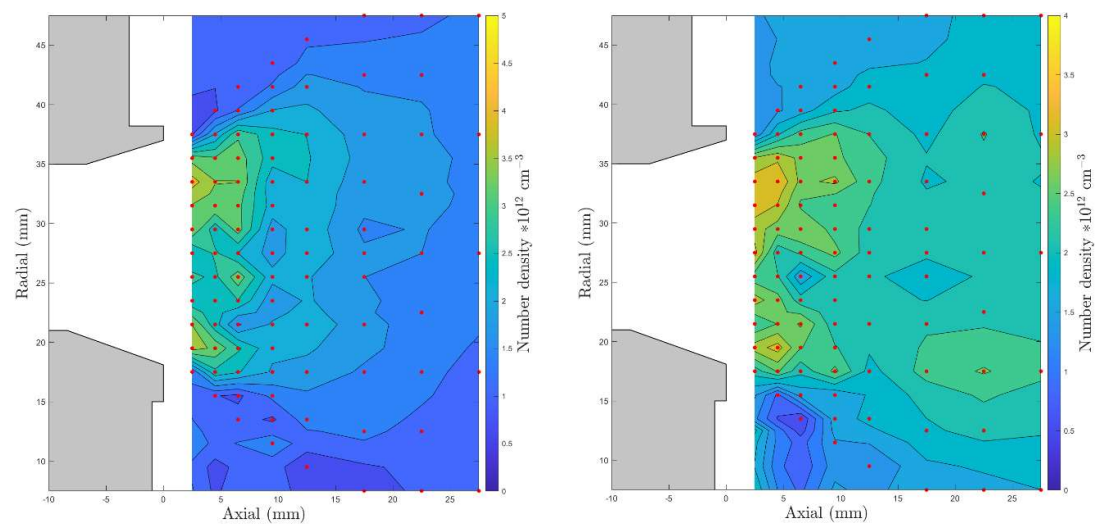


Figure 12. Left - Neutral density map from anode flow on the side opposite the cathode assembly at 540 W, 30 μTorr (condition 3). Right - Neutral density map from anode flow on the side opposite the cathode assembly at 540 W, 60 μTorr (condition 4).

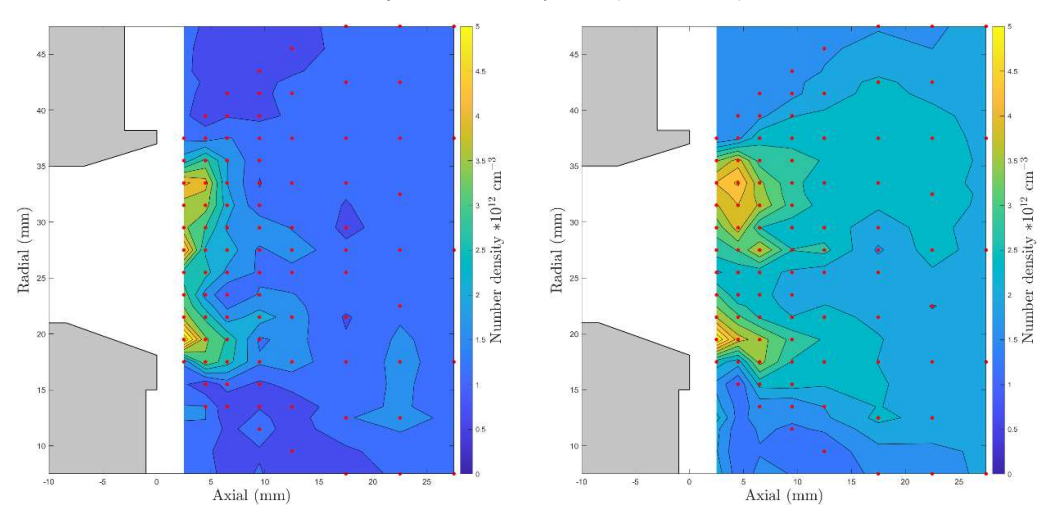


Figure 13. Left - Neutral density map from anode flow on the side opposite the cathode assembly at 720 W, 36 μTorr (condition 5). Right - Neutral density map from anode flow on the side opposite the cathode assembly at 720 W, 60 μTorr (condition 6).

The influence of background pressure on the measured density distributions is evident when comparing low- and high-pressure conditions. The low-pressure maps, shown in the left panels of Figs. 12 and 13, exhibit significantly more detailed spatial structure with sharper gradients and well-defined features, while the high-pressure conditions show smoother, more diffuse density distributions. This behavior is expected given that elevated background pressure effectively bathes the entire measurement domain in higher neutral density, which tends to obscure the sharp gradients and fine-scale structure that are readily apparent under low pressure conditions. Additionally, the hole in the middle of the expansion region, due to ionization, has higher densities in the high-pressure conditions than the corresponding low-pressure conditions. This is an indication of background neutral particles being ingested by the thruster, which is the well-established explanation for the apparent increase in thruster efficiency at higher background pressures.

As can be seen in Fig. 14, additional measurements collected on the cathode side of the thruster under low pressure conditions for both power levels reveal important asymmetries in the neutral distribution across the thruster face. While both sides of the thruster exhibit similar fundamental features—specifically the characteristic double-



pronged structure with a central low-density region—significant differences are observed in the spatial extent of these features. Most notably, the outer prong on the cathode side extends much further downstream, reaching 15-20 mm beyond the exit plane compared to approximately 5 mm on the non-cathode side. This extended neutral distribution results from the interaction between cathode flow and the primary anode discharge, where neutrals supplied by the cathode assembly mix with and modify the expansion characteristics of the main propellant flow.

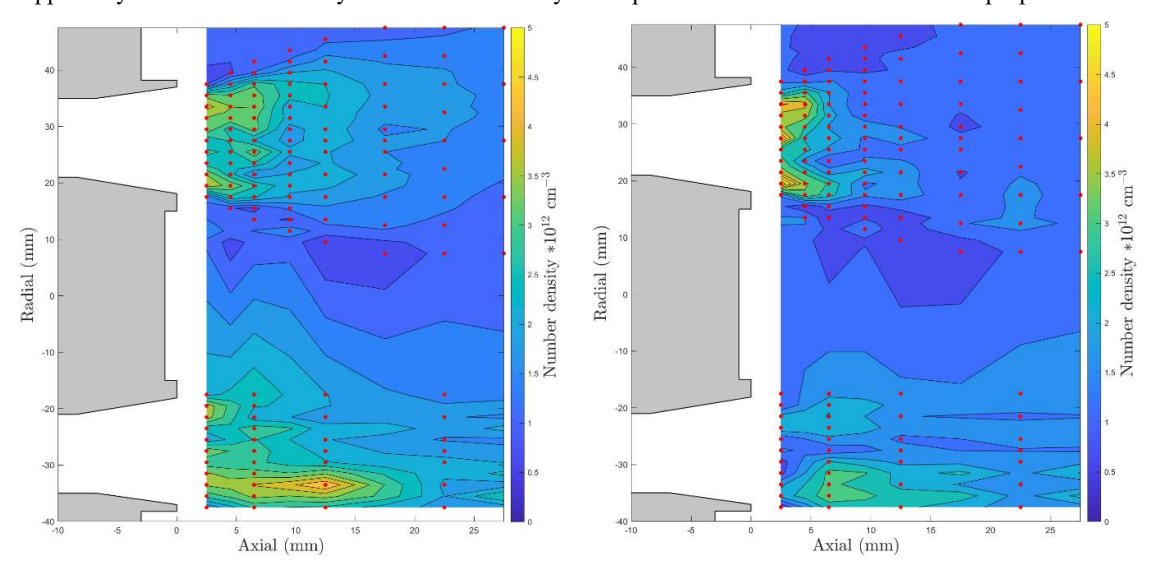


Figure 14. Left – Neutral density map from anode flow on the side opposite the cathode assembly at 540 W, 30 μTorr (condition 3). Right – Neutral density map from anode flow on the side opposite the cathode assembly at 720 W, 36 μTorr (condition 5).

Figs. 15 and 16 present the spatial maps of the standard deviation in neutral number density for the four operating conditions tested, with Fig. 15 corresponding to the 540 W cases at low and high pressure, and Fig. 16 corresponding to the 720 W cases at low and high pressure. Across all operating conditions, the error maps exhibit similar qualitative trends. At the periphery of the near-field plume, further downstream and toward the outer edges, the relative error is approximately 20%. This represents an order of magnitude increase compared to the uncertainty observed in cold flow testing. The elevated error levels in the plume environment are primarily attributed to the reduced neutral density available to probe, as well as the higher plasma luminosity, which constrains the detector gain and introduces additional noise into the TALIF measurements. Another key contributor to the elevated uncertainty is the presence of the breathing mode oscillation in the thruster, which modulates the neutral density on a timescale comparable to the laser pulse repetition. Since TALIF captures traces at arbitrary phases of this oscillation, the resulting measurements effectively average over a strongly varying signal, further increasing the apparent standard deviation. Incorporating time-resolved diagnostics would provide a pathway to separating these oscillations from the mean signal and thereby reducing the uncertainty.

Closer to the thruster exit plane and towards the centerline of the thruster, the measurement uncertainty worsens significantly, with relative errors on the order of 100% in some regions. While the neutral density magnitudes in these regions are similar to those at the outer edges, the background plasma emission is considerably more intense near the thruster exit. This severely limits the achievable detector gain, amplifying noise and reducing sensitivity to the TALIF signal. Combined with the strong influence of the breathing mode, the result is substantial variability in the measured neutral density. These findings emphasize the challenges of measuring neutrals in the near-field of operating Hall thrusters and highlight the need for advanced approaches, such as time-resolved TALIF and gated detection strategies, to better resolve the oscillatory dynamics and improve the fidelity of neutral density measurements in high-luminosity plasma environments.



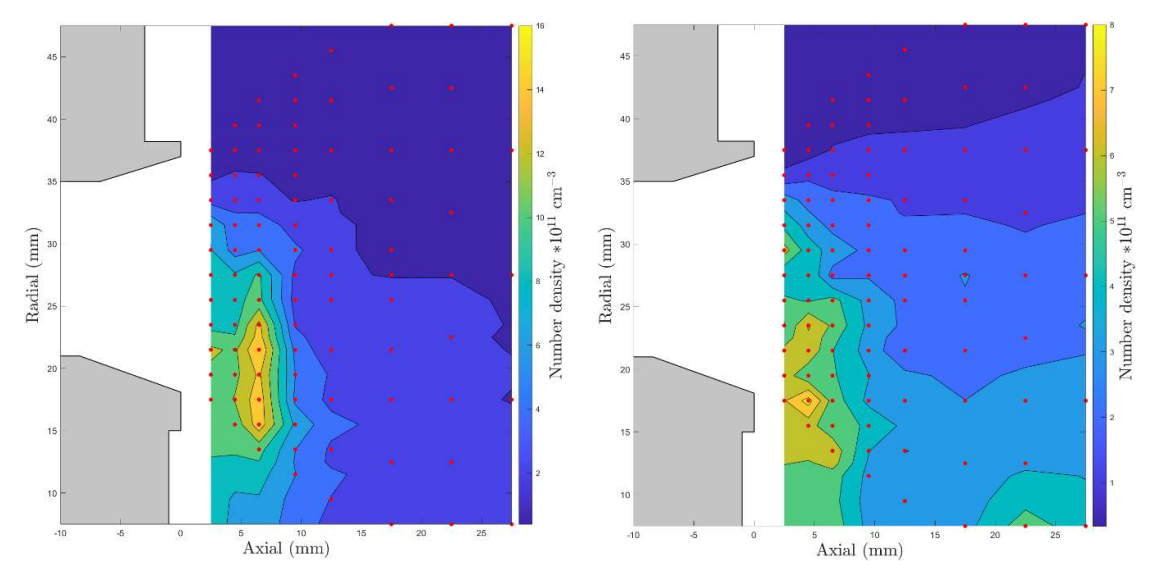


Figure 15. Left - Standard deviation in measurements of anode cold flow map reported in number density at 540 W, 30 μTorr (condition 3). Right - Standard deviation in measurements of anode cold flow map reported in number density at 540 W, 60 μTorr (condition 4).

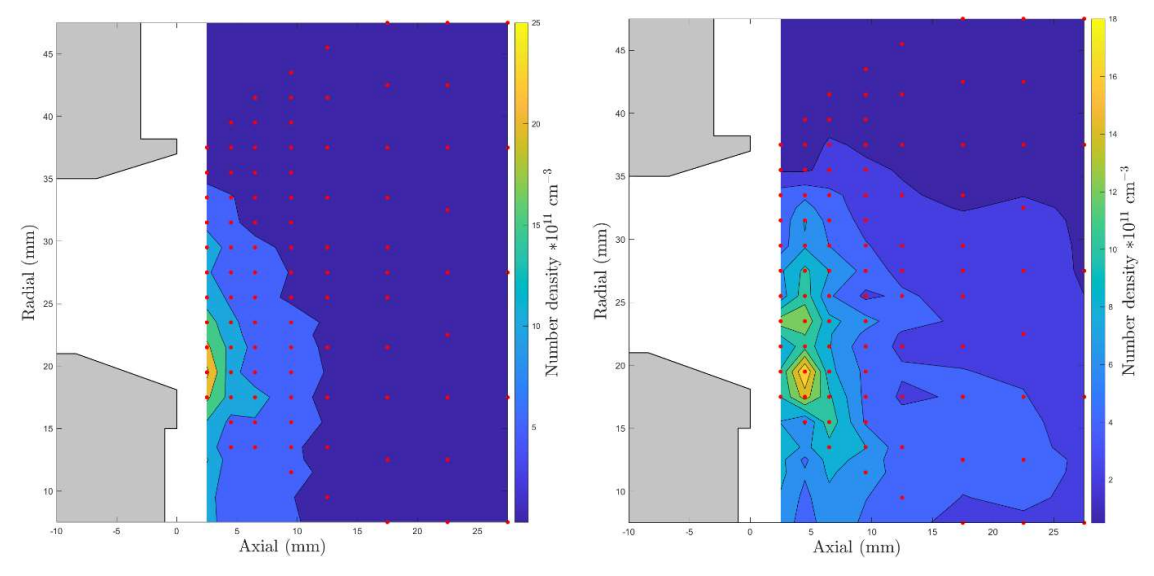


Figure 16. Left - Standard deviation in measurements of anode cold flow map reported in number density at 720 W, 36 µTorr (condition 5). Right - Standard deviation in measurements of anode cold flow map reported in number density at 720 W, 60 µTorr (condition 6).

IV. Conclusions and Future Work

In this work, we applied TALIF to produce high-resolution spatial maps of the neutral density in the near field of the SPT-70 Hall thruster. Measurements were performed across four operating conditions to evaluate how discharge power and facility background pressure influence neutral distributions, with additional comparisons to cold flow operation. These results provide new insight into the role of operating parameters in shaping the neutral environment of a Hall thruster, which is critical for understanding both performance and lifetime.

In addition to mapping neutral densities, we also conducted tests to better quantify the inherent systematic errors in our experimental setup. Based on these evaluations, we estimate a systematic uncertainty of approximately $\sim 20\%$ due to instrumental effects. As part of this effort, we established a correction technique to compensate for slow drifts in laser performance. Without this correction, such drifts would manifest as additional uncertainty in the measured densities. Together, these steps strengthen the reliability of the TALIF measurements and provide a framework for future high-accuracy experiments.



Looking forward, there are several clear pathways for improving both the diagnostic fidelity and efficiency of the TALIF setup. Here is a list of the improvements:

- Introduce gating circuit for PMT enables higher gain to improve SNR.
- Reduce collection optics radius possibly reduces background luminosity collection more than signal.
- Implement narrower bandpass filter further rejects nearby emission lines being let through by the current bandpass filter.
- Employ time-resolved TALIF techniques removes uncertainty due to averaging over breathing mode.
- Upgrade the wavemeter gives better resolution for wavelength stabilization.
- Automate the TALIF diagnostic improve collection times and labor required to collect maps.

These improvements would permit studies on higher powered and more innovative thruster technologies.

Appendix

Systematic Error Estimation Results

Test 1 – Neutral Distribution Homogeneity Assessment at Reference Location: This experiment evaluated the spatial uniformity of neutral particle density at the reference calibration location and investigated whether different gas injection points created systematic variations in the local neutral environment. With the chamber maintained at a constant background pressure of 1.2×10⁻⁴ Torr, krypton gas was sequentially introduced through two distinct pathways: the thruster anode and the dedicated bleed line located behind the thruster. At both injection configurations, TALIF signals were recorded at the reference measurement location, and additional measurements were taken at nearby spatial positions to map any local density gradients. This test was designed to verify the fundamental assumption that the reference location experiences a homogeneous neutral density field regardless of the gas source, and to identify whether different injection geometries create preferential flow patterns or localized density enhancements that could introduce systematic errors in the absolute calibration.

When krypton gas was sequentially injected through the two pathways (thruster anode and bleed line), there was a discrepancy between the measured TALIF signals at the reference location. Flowing through the anode produced about a 50% higher signal for a given background pressure as measured by the ion. We proceeded with performing the calibration measurements with the bleed line as we assumed the increased distance from the measurement location would allow for a more homogenous mixing of the background gas. Additionally, when the measurement location was moved within a 3 mm radius around the nominal reference position, no measurable change in signal was observed, demonstrating that measurements were being conducted in a spatially homogeneous region.

Test 2 – Drift Correction Validation/Quantification: This experiment characterized the performance and limitations of the temporal drift correction algorithm under idealized measurement conditions without the additional complexities introduced by thruster operation. The TALIF system was positioned at a fixed location within the cold-flow neutral expansion from the thruster, and continuous measurements were acquired over several hours while implementing the standard reference point monitoring procedure. By conducting this extended measurement campaign in the absence of thruster-induced plasma effects, background luminosity, and thermal instabilities, this test isolated the intrinsic accuracy of the counter-drift technique and quantified the residual measurement uncertainties attributable solely to laser wavelength drift and optical system variations. The multi-hour duration provided sufficient statistical sampling to assess both short-term measurement repeatability and long-term systematic trends.

Fig. 17 illustrates the performance of the drift correction algorithm under controlled conditions. The left panel shows the temporal evolution of the photodiode energy signal throughout the measurement campaign, with the yellow line specifically highlighting the signals values recorded at the reference measurement points. The right panel displays the corresponding evolution of the ratio between the TALIF signal and the photodiode signal, normalized against the energy measurement, with the yellow line emphasizing the ratios obtained at the reference points. This allows for visualization of the two drifts, laser energy and wavelength drift.



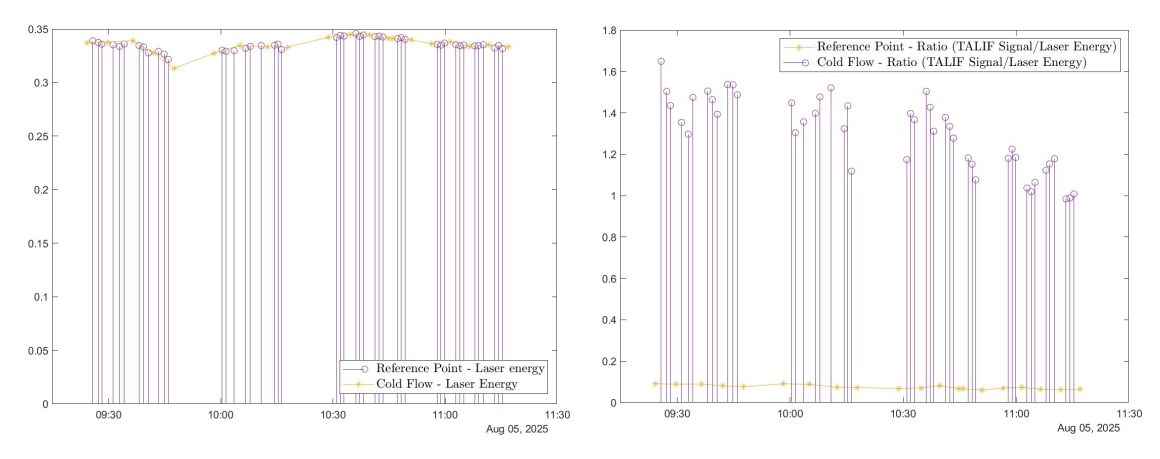


Figure 17. Left - The time evolution of laser energy at fixed location in cold flow. Right – The time evolution of the ratio of TALIF signal and laser energy at fixed location in cold flow.

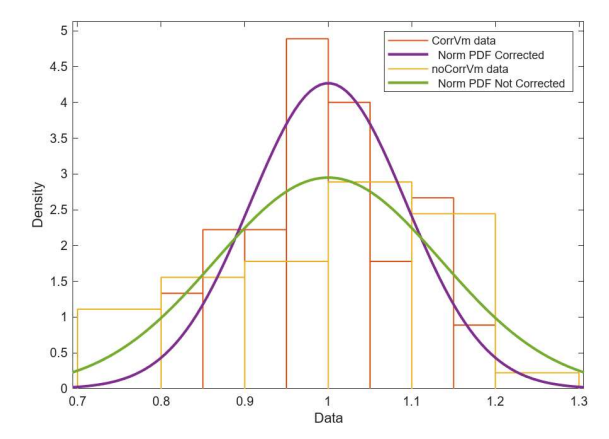


Figure 18. Histogram and corresponding probability distribution function (PDF) of the uncorrected data with the corrected data overlayed.

The drift correction algorithm operates by applying a linear scaling factor that forces the blue reference point line to maintain a constant value across time, effectively removing the temporal variations, and then interpolating this correction linearly to all TALIF measurements acquired between consecutive reference points. Fig. 18 presents histograms comparing the corrected and uncorrected datasets along with their respective overlaid PDFs, demonstrating a significant improvement in measurement precision from 14% standard deviation in the raw data to 9% standard deviation after applying the drift correction methodology.

This test established the baseline performance of the drift correction algorithm under ideal conditions, representing the best-case scenario performance before additional error sources from thruster operation are introduced.

Test 3 – Thruster Operating Condition Repeatability: This experiment evaluated the reproducibility of neutral density measurements under varying thruster operating conditions and investigated the stability of plasma discharge influences on the local neutral environment. The TALIF system was positioned at a fixed measurement location within the thruster plume that provided adequate signal-to-noise ratio while avoiding regions with steep spatial gradients that could amplify positioning uncertainties.

The thruster was operated at two distinct power levels (540 W and 720 W), with systematic variations in background pressure introduced by modulating the krypton flow rate through the feedline. At the initial 540 W condition, the background pressure was cycled between 30 μ Torr and 60 μ Torr. For each setpoint, three consecutive 500-shot TALIF measurements were acquired after allowing three minutes for thruster stabilization following each pressure change. This pressure cycle was repeated twice to assess short-term repeatability. The power was then increased to 720 W with the background pressure set to 36 μ Torr, giving the thruster approximately 20 minutes for thermal and discharge stabilization. Similar pressure cycling between 36 μ Torr and 60 μ Torr was then performed. The entire experimental sequence was repeated to evaluate longer-term reproducibility.



Cycling the pressure did not produce significant changes in the measured neutral density values. The standard deviation between cycles of measurements was comparable to the 500-shot standard deviation at a given measurement location. This trend held true across both thruster operating conditions.

When analyzing standard deviation behavior in more detail, the low-power, low-pressure condition exhibited little variation: the percent standard deviation remained near 25% even after repeated condition changes. Under the low-power, high-pressure condition, however, the percent standard deviation shifted from ~6% to ~8%. Because this absolute error level was much smaller, the change is attributed to the drift correction algorithm rather than thruster repeatability. At high power, both low- and high-pressure conditions yielded errors of ~19%, with negligible changes across repeated cycles.

Although the error did not vary substantially during this test, the results provide only preliminary indications of measurement repeatability under realistic thruster operating conditions with plasma effects present. The experiment quantified the uncertainty associated with operational variations and suggested that neutral density profiles may remain consistent when returning to nominally identical discharge conditions. However, the limited number of operating points, relatively small sample size, and restricted duration of testing preclude drawing firm conclusions. A longer-term, systematically designed study will be required to rigorously establish the reproducibility of neutral density measurements across a broader range of thruster conditions.

Test 4 – Spatial Positioning Uncertainty: This diagnostic assessment quantified the systematic displacement of measurement locations relative to the thruster assembly that occurred during vacuum chamber operation. The spatial uncertainty arose from mechanical deformation of the vacuum chamber when transitioning from atmospheric to operating pressure conditions. Since the thruster was mounted to the chamber door via the thrust stand, the structural deflection under vacuum loading caused a measurable shift in the relative positioning between the TALIF measurement system and the thruster assembly. This displacement was attributed to door deflection under vacuum loading, with the assumption that lateral (radial) positioning remained unaffected due to the symmetric nature of the chamber deformation. To validate this assumption and confirm that radial alignment was preserved, optical back-illumination was employed whereby light was transmitted in reverse through the collection optics and its intersection point with specific features on the thruster hardware was visually confirmed.

The positioning uncertainty analysis revealed a consistent axial displacement of 2.5±0.5 mm upstream from the original alignment positions under vacuum conditions. This displacement was attributed to door deflection under vacuum loading, with lateral (radial) positioning remaining unaffected due to the symmetric nature of the chamber deformation. Optical back-illumination validation confirmed that radial alignment was preserved. This positioning uncertainty represents a fundamental systematic error source that must be incorporated into the spatial resolution and uncertainty analysis of all plume mapping measurements, particularly when comparing data across different chamber pressure conditions or when precise spatial registration is critical for gradient calculations.

The comprehensive series of systematic error characterization tests provided crucial insights into the various uncertainty sources affecting the absolute neutral density measurements. Test 1 confirmed the spatial homogeneity of the reference calibration region and validated the independence of the calibration from gas injection methodology. Test 2 established the baseline performance of the drift correction algorithm under ideal conditions, while Test 3 demonstrated the repeatability of measurements under realistic thruster operating conditions with plasma effects present. Test 4 quantified the mechanical positioning uncertainties inherent to the vacuum chamber operation.

Acknowledgements

This work was supported by NASA through the Joint Advanced Propulsion Institute (JANUS), a NASA Space Technology Research Institute, grant number 80NSSC21K1118. Special thanks to the AFRL/RQRS for loan of the SPT-70.

References

- [1] Goebel, D. M., and Katz, I., "Fundamentals of Electric Propulsion Ion and Hall Thrusters." Retrieved 12 September 2023. https://descanso.jpl.nasa.gov/SciTechBook/st_series1_chapter.html
- [2] Mazouffre, S., "Electric Propulsion for Satellites and Spacecraft: Established Technologies and Novel Approaches," Plasma Sources Science and Technology, Vol. 25, No. 3, 2016, p. 033002. https://doi.org/10.1088/0963-0252/25/3/033002
- [3] Choueiri, E. Y., "Plasma Oscillations in Hall Thrusters," *Physics of Plasmas*, Vol. 8, No. 4, 2001, pp. 1411–1426. https://doi.org/10.1063/1.1354644



- [4] Walker, M. L. R., "Effects of Facility Backpressure on the Performance and Plume of a Hall Thruster.," Thesis. 2005.
- [5] Walker, M. L. R., and Gallimore, A. D., "Performance Characteristics of a Cluster of 5-kW Laboratory Hall Thrusters," *Journal of Propulsion and Power*, Vol. 23, No. 1, 2007, pp. 35–43. https://doi.org/10.2514/1.19752
- [6] Reid, B. M., "The Influence of Neutral Flow Rate in the Operation of Hall Thrusters."
- [7] Crofton, M., "Measurement of Neutral Xenon Density Profile in an Ion Thruster Plume," 27th Plasma Dynamics and Lasers Conference, American Institute of Aeronautics and Astronautics. https://doi.org/10.2514/6.1996-2290
- [8] Eichhorn, C., Pietzonka, L., Scholze, F., Bundesmann, C., Spemann, D., Neumann, H., and Leiter, H. J., "Single-and Two-Photon Absorption Laser-Induced Fluorescence Spectroscopy in Rare Gases for Gridded Ion Thruster Diagnostics," *EPJ Techniques and Instrumentation*, Vol. 9, No. 1, 2022, pp. 1–20. https://doi.org/10.1140/epjti/s40485-022-00077-y
- [9] Eichhorn, C., Winter, M., Auweter-Kurtz, M., and Löhle, S., "Multi-Photon Spectroscopy on Xenon for Application on Ion Thruster Plasma Parameter Investigations: Experiment and Theory | Request PDF." Retrieved 22 May 2024. https://www.researchgate.net/publication/242186221_Multi-Photon_Spectroscopy_on_Xenon_for_Application_on_Ion_Thruster_Plasma_Parameter_Investigations_Experimen t and Theory
- [10] Eichhorn, C., Winter, M., Auweter-Kurtz, M., and Löhle, S., "Theoretical and Experimental Approach of Multi-Photon Spectroscopy on Xenon for Application on Ion Thruster Plasma Parameter Investigation," 38th Plasmadynamics and Lasers Conference, American Institute of Aeronautics and Astronautics, 2007. https://doi.org/10.2514/6.2007-3878
- [11] Crofton, M., Hsu Schouten, A., Young, J., Beiting, E., Diamant, K., Corey, R., and Delgado, J., "Neutral Xenon Density in the SPT-140 Near-Field Plume," presented at the International Electric Proulsion Conference, 2013.
- [12] Gottfried, J., Antozzi, S., Dumitrache, C., and Yalin, A. P., "Preliminary Krypton Measurements by Two-Photon Absorption Laser Induced Fluorescence (TALIF) in Cold Flow and a Hollow Cathode Plasma," *AIAA SCITECH 2023 Forum*, American Institute of Aeronautics and Astronautics. https://doi.org/10.2514/6.2023-1863
- [13] Antozzi, S., Gottfried, J., Williams, J. D., and Yalin, A. P., "Spatially Resolved Measurements of Krypton by Two-Photon Absorption Laser Induced Fluorescence (TALIF) in a Barium Oxide Hollow Cathode Plasma," AIAA AVIATION 2023 Forum, American Institute of Aeronautics and Astronautics. https://doi.org/10.2514/6.2023-4269
- [14] Wegner, J. T., "Two-Photon Absorption Laser Induced Fluorescence (TALIF) of Neutral Xenon in a Hall Effect Thruster Plasma," M.S. Colorado State University, United States -- Colorado, 2021.
- [15] Gottfried, J. A., Antozzi, S., Stienike, J., Thompson, S. J., Williams, J. D., and Yalin, A. P., "Temporally Resolved Relative Krypton Neutral Density during Breathing Mode of a Hall Effect Thruster Recorded by TALIF," *Journal of Electric Propulsion*, Vol. 3, No. 1, 2024, p. 9. https://doi.org/10.1007/s44205-024-00070-5
- [16] Dale, E. T., and Jorns, B. A., "Experimental Characterization of Hall Thruster Breathing Mode Dynamics," *Journal of Applied Physics*, Vol. 130, 2021, p. 133302. https://doi.org/10.1063/5.0046048
- [17] Dale, E., and Jorns, B., "Two-Zone Hall Thruster Breathing Mode Mechanism, Part II: Experiment," 2019.

